

# Journal of Biomedical Optics

[SPIEDigitalLibrary.org/jbo](http://SPIEDigitalLibrary.org/jbo)

## **Trends in melanosome microcavitation thresholds for nanosecond pulse exposures in the near infrared**

Morgan S. Schmidt  
Paul K. Kennedy  
Rebecca L. Vincelette  
Michael L. Denton  
Gary D. Noojin  
Kurt J. Schuster  
Robert J. Thomas  
Benjamin A. Rockwell

# Trends in melanosome microcavitation thresholds for nanosecond pulse exposures in the near infrared

Morgan S. Schmidt,<sup>a,\*</sup> Paul K. Kennedy,<sup>a</sup> Rebecca L. Vincelette,<sup>b</sup> Michael L. Denton,<sup>b</sup> Gary D. Noojin,<sup>b</sup> Kurt J. Schuster,<sup>b</sup> Robert J. Thomas,<sup>a</sup> and Benjamin A. Rockwell<sup>a</sup>

<sup>a</sup>711th Human Performance Wing, Human Effectiveness Directorate, Bioeffects Division, Optical Radiation Branch, 4141 Petroleum Road, JBSA, Fort Sam Houston, Texas 78234

<sup>b</sup>TASC Inc., 4241 Woodcock Drive, Suite B-100, San Antonio, Texas 78228

**Abstract.** Thresholds for microcavitation of bovine and porcine melanosomes were determined using nanosecond laser pulses in the near-infrared (1000 to 1319 nm) wavelength regime. Isolated melanosomes were irradiated by single pulses (10 or 50 ns) using a Q-switched Spectra Physics Nd:YAG laser coupled with an optical parametric oscillator (1000 to 1200 nm) or a continuum laser at 1319 nm. Time-resolved nanosecond strobe photography after the arrival of the irradiation beam allowed imaging of microcavitation events. Average fluence thresholds for microcavitation increased nonlinearly with increasing wavelength from  $\sim 0.5 \text{ J/cm}^2$  at 1000 nm to  $2.6 \text{ J/cm}^2$  at 1319 nm. Fluence thresholds were also measured for 10-ns pulses at 532 nm and found to be comparable to visible nanosecond pulse values published in previous reports. Calculated melanosome absorption coefficients decreased from  $925 \text{ cm}^{-1}$  at 1000 nm to  $176 \text{ cm}^{-1}$  at 1319 nm. This trend was found to be comparable to the decrease in retinal pigmented epithelial layer absorption coefficients reported over the same wavelength region. Estimated corneal total intraocular energy retinal damage threshold values were determined in order to compare to current and proposed maximum permissible exposure (MPE) safe levels. Results from this study support recently proposed changes to the MPE levels. © The Authors. Published by SPIE under a Creative Commons Attribution 3.0 Unported License. Distribution or reproduction of this work in whole or in part requires full attribution of the original publication, including its DOI. [DOI: [10.1117/1.JBO.19.3.035003](https://doi.org/10.1117/1.JBO.19.3.035003)]

Keywords: microcavitation; laser safety; melanosome; retinal pigment epithelium; damage threshold; maximum permissible exposure.

Paper 130826R received Nov. 19, 2013; revised manuscript received Jan. 28, 2014; accepted for publication Feb. 3, 2014; published online Mar. 10, 2014.

## 1 Introduction

As a consequence of the widespread use and availability of lasers, laser eye safety has increasingly become a concern due to the possibility of accidental, high-intensity exposures to tissue in the eye. The American National Standards Institute (ANSI) accredits the Z136 committee to establish user standards for the safe use of lasers. In order for committees such as Z136 to monitor and make recommendations for safe exposure levels,<sup>1,2</sup> retinal damage threshold studies must be conducted with varying laser radiation parameters to quantify the magnitude of these hazards.<sup>3</sup> It is also imperative to understand the mechanisms of retinal damage, including melanosome microcavitation, as a function of wavelength, spot size, and exposure duration. Furthermore, the ANSI Z136.1 in the United States is currently under revision. The proposed revision to the near-infrared (NIR) safe exposure limits is supported by ocular damage threshold data from a number of studies.<sup>3,4</sup> However, little data exist in the longer-wavelength NIR regime in the nanosecond time scale. An additional barrier to updating the laser safety standards is the lack of understanding of the fundamental damage mechanisms of melanosome microcavitation in the retinal pigment epithelium (RPE) in this time regime.

Therefore, the objective of this study was to investigate the trends in single-melanosome microcavitation thresholds for nanosecond pulse exposures in the NIR wavelength regime. Average fluence thresholds for microcavitation of isolated bovine and porcine melanosomes were determined using nanosecond laser pulses with wavelengths ranging from 1000 to 1319 nm. A tunable laser source was used in order to probe NIR wavelengths of interest. Both heavy and light melanosome fractions for bovine and porcine were studied to determine if the threshold varied as a function of melanosome shape. An additional purpose of this study was to investigate whether or not melanosome microcavitation is maintained as the dominant damage mechanism with increasing wavelength throughout the retinal hazard regime, commonly identified as  $\sim 400$  to 1400 nm. For nanosecond and picosecond pulse exposures, microcavitation about heated melanosomes, producing bubble formation and shock wave emission, is believed to be the dominant threshold-level retinal damage mechanism.<sup>5-10</sup>

This study focuses on the wavelength dependence of melanosome microcavitation damage thresholds over the 1000 to 1319 nm transition wavelength region. Results of this study were compared to the current ANSI Z136.1-2007 maximum permissible exposure (MPE) values, the proposed (201x) MPE values, as well as *in vivo* studies. These results will provide critical information supporting an update of laser safety standards, and provide evidence in support of a proposal to increase the exposure limits in the NIR wavelength region in the 1000 to 1319 nm range.<sup>4</sup>

\*Address all correspondence to: Morgan S. Schmidt, E-mail: [mssschmidt@gmail.com](mailto:mssschmidt@gmail.com)

## 2 Background

### 2.1 Retinal Pigment Epithelium and Melanosomes

The retina is a visual organ of  $\sim 300 \mu\text{m}$  thickness located in the back of the eye.<sup>11</sup> The RPE is a monolayer of cells located within the retina. Melanin-containing organelles known as melanosomes, found in RPE cells, readily absorb  $\sim 50$  to  $60\%$  of the incident visible light as well as NIR radiation.<sup>5,11,12</sup> For visible laser exposures, injury first occurs in the RPE because it contains the highest energy density of absorbed photons. As wavelength increases from the visible to the NIR, laser light is absorbed less in the retina and more in the cornea and anterior segments of the eye.<sup>3,13,14</sup> In addition, as melanin absorption significantly decreases, water absorption increases with wavelength. The heat produced by the strongly absorbing melanosomes in the RPE exposed to visible and NIR nanosecond pulses allows for selective damage of RPE cells while preserving overlying photoreceptors.<sup>12,15</sup>

### 2.2 Mechanisms of Short-Pulsed Laser-Induced Retinal Injury

Numerous ocular bioeffect experiments have been performed using lasers in the wavelength region between 1000 and 1300 nm with many different pulse durations.<sup>3,4,16–18</sup> Additional threshold measurements were made on an artificial retina for a variety of wavelengths, spot sizes, and pulse durations to reduce the complications of a biological system.<sup>19</sup> However, except for Nd:YAG (1064 nm) bioeffect studies, little experimental data exist in this wavelength region using very short-pulse durations (order of nanoseconds). When laser pulses shorter than  $20 \mu\text{s}$  impinge on the retina, heating is confined to the absorbing melanosome during the laser exposure (thermal confinement). The temperature rise and threshold for injury is dependent on the number density of absorbed photons.<sup>20</sup>

Birngruber et al.<sup>14</sup> defined the relationship between the spatial temperature equilibration of melanin granules and the space between them, expressed as the thermal relaxation time ( $\tau_R$ ) for a particle.

$$\tau_R = r^2/6\kappa, \quad (1)$$

where  $r$  is the intergranule distance and  $\kappa$  is the thermal diffusivity. By using the thermal diffusivity of water ( $\kappa = 1.5 \times 10^{-7} \text{ m}^2 \text{ s}^{-1}$ ), and a distance of  $1.2 \mu\text{m}$ , an upper limit for the thermal relaxation time of  $\sim 1 \mu\text{s}$  results from Eq. (1).<sup>14</sup> The thermal relaxation time of melanosomes has also been expressed as

$$\tau_R = r^2/4\kappa, \quad (2)$$

where  $\kappa = 1.4 \times 10^{-7} \text{ m}^2 \text{ s}^{-1}$  is the thermal diffusivity of melanosomes.<sup>6,21,22</sup> Equation (2) results in a thermal relaxation time of  $\sim 450 \text{ ns}$ , using a melanosome radius of  $0.5 \mu\text{m}$ .<sup>6,7</sup> Therefore, the range of thermal relaxation time of melanosomes is  $\sim 450 \text{ ns}$  to  $1 \mu\text{s}$ . If heat is generated within an absorbing target more rapidly than heat can diffuse away, high temperatures can be obtained, leading to vaporization of the surrounding fluid when exposures are above the microcavitation threshold.<sup>6</sup> One can assume spatially homogeneous heat deposition occurs within the particle if the thermal relaxation

time of the particle is much smaller than the laser pulse duration.

This process results in the formation of small bubbles (microcavitation) around laser-heated melanosomes, which may cause damage to the surrounding tissue.<sup>23</sup> When these microcavitation bubbles expand and collapse, they break the cell membrane and destroy the cell.<sup>8,24</sup> However, melanosome microcavitations may not always lead to cell death. Gerstman et al. developed expressions for calculating the size of microcavitation bubbles as a function of laser fluence and melanosome properties, including radius and absorptivity.<sup>10</sup> These authors showed that the maximum bubble radius can significantly change, and the treatment of bubble formation and growth may be used to analyze threshold damage leading to lesions and cell death. Therefore, the microcavitation events must be large enough to impact the cell membrane in order to cause cell death.

It has been observed that the transition from thermal damage to bubble-induced damage from single pulses occurs at  $\sim 5 \mu\text{s}$  in duration.<sup>7,11,25</sup> Studies have also shown that the microcavitation thresholds decrease with increasing number of pulses.<sup>26</sup> The RPE is believed to be the site for threshold damage for all nanosecond and picosecond laser exposures in the visible and NIR. In the NIR wavelength region, the ocular media and anterior structures of the eye (cornea and lens) begin to strongly absorb, but still transmit adequate energy to pose a risk to the retina.<sup>3</sup> At some wavelength, either bulk (water) heating around the melanosomes will take over as the threshold damage mechanism or the absorption in the anterior segment of the eye becomes dominant and the cornea or lens will be damaged.<sup>9</sup> The viscoelastic properties of the medium in which a sample is prepared in have additional effects on bubble formation. Studies have shown that the observation and formation of cavitation bubbles can vary greatly depending on the surrounding medium.<sup>27,28</sup> The surrounding media for the present study is water for all cases.

## 3 Experimental Detail and Procedures

### 3.1 Melanosome Preparation

The preparation procedure of bovine and porcine pigment granules (melanosomes) followed the method of Dontsov et al.<sup>29</sup> This method provided samples enriched in light and heavy fractions of melanosomes by density for both bovine and porcine samples. Light melanosomes are predominately spherical, while the heavy melanosomes are predominately elliptical in shape, resulting in slight size differences between the two fractions.<sup>26,29</sup> However, no high-resolution imaging was used, and therefore, no precise knowledge of shape variance within each fraction was obtained. The melanosome fractions were separated in order to determine if differences in microcavitation threshold values occur. After the separation procedure, stock solutions of the melanosomes were stored at  $4^\circ\text{C}$ . Dilutions of samples were prepared in deionized water for each fraction prior to analysis. Plated aqueous melanosomes were prepared on glass microscope slides in order to observe cavitation events. A loosely sealed silicon washer and glass cover slip were used to enclose the melanosome sample to prevent evaporation of the aqueous suspension. By plating samples on a clear glass slide, observations of the microcavitation events were made possible using a camera positioned below the sample suspension and strobe back-illumination.

### 3.2 Laser and Optical Systems

In order to observe the microcavitation events after exposure, a microscope containing two beam paths was used (see Fig. 1): (1) the irradiation beam and (2) the illumination beam. It was necessary to use two different laser systems for collection of microcavitation data in the wavelength region of 1000 to 1300 nm. First, the irradiation beam consisted of a Spectra Physics Pro 290, Nd:YAG with an output of 300 mJ at 355 nm, coupled with a nanosecond optical parametric oscillator (OPO) laser (Spectra Physics, Santa Clara, California, Premiscan), with a wavelength output range of 240 nm to 2.4  $\mu\text{m}$ . This system was used for data collection in the 1000 to 1200 nm wavelength region and had a pulse duration of 10 ns. A half-wave-plate and polarizing cube controlled the pulse energy delivered to the sample. A Coherent-Moletron EMP2000 energy meter (Coherent, Inc., Santa Clara, California) collected energy measurements. A beam splitter (BS) directed 10% of the beam energy into a reference detector (P1), and the remaining energy passed through the splitter and was measured by a second energy detector (P2) at the sample site. The ratio between the two detectors was measured and recorded before every experimental run. After each shot, the pulse energy from P1 was multiplied by the P1/P2 ratio to determine the energy delivered to the sample. The P1/P2 ratio was monitored during data collection and was stable throughout each data series. Data collection occurred at 1000, 1100, and 1200 nm.

In order to collect data at 1319 nm, a custom-built Q-switched Nd:YAG laser (Continuum Lasers, Santa Clara, California) was

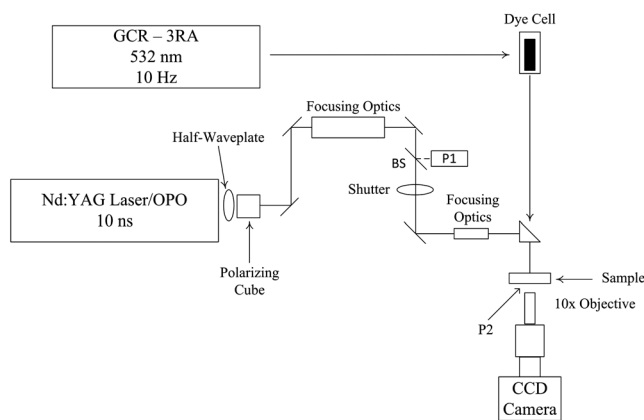


**Fig. 1** Schematic of the laser and illumination setup for observing microcavitation bubble formation from irradiated melanosomes. BS, a beam splitter, directed 10% of the beam energy into P1, a reference energy meter. P2, a detector, measured the remaining energy that passed through the BS at the sample site.

used to deliver 50-ns exposures to the melanosomes, instead of the OPO's 10-ns exposures. This laser delivers high-power pulses at 1319 nm and provided enough energy for microcavitation. The maximum pulse energy of the laser was rated at 5 J; however, for this experiment, only one of the nine amplifier stages was used. A third source, a frequency-doubled 1064 nm Q-switched Nd:YAG laser (Spectra Physics, INDI-30) was used to collect microcavitation data at 532 nm. The pulse duration of this system was 10 ns.

The illumination beam consisted of a Spectra Physics Model GCR-130 Nd:YAG and was frequency doubled for an output of 532 nm at 10 Hz. The GCR-130 output was directed through a dye cell containing Rhodamine 640 Perchlorate dissolved in methanol. The dye absorbed the 532-nm energy and emitted at  $\sim 620$  nm. The fluorescence of the dye cell was collected at 90 deg to the GCR-130 and directed to the sample. The illumination beam was directed to the sample through the back of an IR mirror that turned the irradiation beam to the sample. A delay generator allowed time-resolved imagery by controlling the delay between the irradiation beam and the illumination beam, as well as triggering the Bobcat CCD camera (Imperx Incorporated, Boca Raton, Florida) to capture an image. The effect of laser light on the melanosomes was observed by a custom-built microscope using a Mitutoyo long-working-distance microscope 10 $\times$  objective (M Plan Apo). A 400-mm tube lens was used in order to achieve a total magnification of 20 $\times$ . This provides micrometer spatial resolution and a nanosecond strobe with steps of nanoseconds relative to the laser illumination. A shutter was placed prior to the sample to collect single-shot data. This setup allowed simultaneous laser irradiation of the melanosomes as well as the observation (photographs) of microcavitation formation. In addition, pre- and postcavitation images were collected and used to background subtract from the exposure image for improved photographs of the cavitation events. Figure 2 shows individual melanosomes under 20 $\times$  magnification [Fig. 2(a)], background-subtracted image of melanosomes during irradiation at 2.0 $\times$  above threshold at 1200 nm [Fig. 2(b)], and background-subtracted image of melanosomes at threshold at 1200 nm [Fig. 2(c)].

## 4 Data Analysis and Threshold Fluence Values

### 4.1 Fluence Threshold Analysis

Beam diameter measurements were determined prior to each data collection set using the knife edge technique. In each case, the spot size consisted of a  $1/e^2$  Gaussian beam, which results in an average fluence value. The NIR exposures (1000 to 1319 nm) had an average beam diameter of  $183 \pm 18 \mu\text{m}$ . Some of the uncertainty in the NIR values is

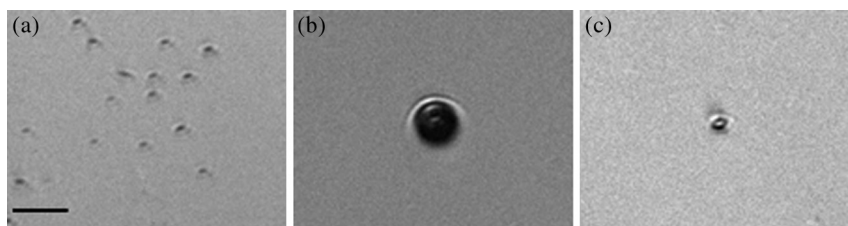


**Fig. 2** (a) Isolated single melanosomes. (b) Cavitation with background subtraction 2.0 $\times$  above threshold. (c) Cavitation with background subtraction at threshold. (b) and (c) are following 1200 nm, 10 ns irradiation. Bar  $\approx 10 \mu\text{m}$ .

due to daily fluctuations from the OPO system. Results indicated no spot-size dependence on threshold fluence values for the small spot size variations in this experiment. Beam diameter measurements were also determined for the 532-nm values, with an average of  $295 \pm 22 \mu\text{m}$ .

The estimated dose for 50% probability of laser-induced damage ( $ED_{50}$ ) was determined through the statistical method of Probit analysis, which is the standard technique for ascribing threshold values.<sup>30,31</sup> The Probit procedure estimated the  $ED_{50}$  fluence required to cause melanosome microcavitation. Binary (yes/no) data points were entered into the Probit software, and the  $ED_{50}$ , slope, and fiducial limits (FL) were determined at the 95% confidence level. The fluence ( $H$ ) is computed by Eq. (3).

$$H = 4Q/\pi D_L^2, \quad (3)$$

where  $Q$  is the energy per pulse and  $D_L$  is the  $1/e^2$  Gaussian beam diameter. In addition, uncertainties in the experimental measurements were taken into account in order to determine the total uncertainty for the fluence values, and resulted in a 16% total uncertainty.

## 5 Results

### 5.1 Threshold Fluence Values for Microcavitation

Using the microscope setup with strobe photography, the microcavitation bubbles were directly visualized and recorded around single melanosomes suspended in deionized water following a single laser pulse. Data collection occurred at 1000, 1100, 1200, and 1319 nm, with 10- or 50-ns pulse duration. In addition, data collection occurred at 532 nm with 10-ns pulse duration to determine if the microcavitation threshold data were comparable to those published by other authors in the visible wavelength regime.<sup>6,20,32</sup> Table 1 summarizes the Probit bovine and porcine microcavitation thresholds for heavy and light melanosome fractions at 1100 nm and includes the upper and lower fiducial limits, Probit slope, and total number of shots per trial. The fiducial limits are based on a 95% confidence interval. In each case, either three or four data sets were collected on different days, and Probit analysis was performed on each data set. These data illustrate that there is no statistical difference between thresholds of bovine and porcine melanosomes. Furthermore, the thresholds for heavy and light fractions within species are not statistically different. Because there were no statistical differences between the light and heavy fractions, all data trials were combined and a single Probit analysis was performed on all the data. Table 2 gives the Probit threshold values for all trials combined and illustrates that the combined trials for each melanosome fraction are statistically equivalent for both bovine and porcine samples at 1100 nm. Table 3 shows the Probit results at 1319 nm using a different laser with 50-ns pulse duration. Because thresholds for both bovine and porcine melanosome fractions were statistically equivalent at each wavelength, these data were later reduced to a single threshold value for each species at 1319 nm as seen in Table 2.

Table 4 summarizes the threshold data for bovine and porcine melanosomes at the four NIR wavelengths. Figure 3 is a plot of the comparison between wavelength and microcavitation threshold from 532 to 1319 nm and illustrates the nonlinear trend of threshold as a function of wavelength. Average fluence thresholds were found to rapidly increase with increasing wavelength from  $0.5 \text{ J/cm}^2$  at 1000 nm to  $2.6 \text{ J/cm}^2$  at 1319 nm. This is

**Table 1** Probit threshold data for a single pulse duration of 10 ns for bovine and porcine heavy (HB, HP) and light fractions (LB, LP) of melanosomes at 1100 nm. The  $1/e^2$  Gaussian beam diameter average was  $183 \mu\text{m}$ . The reported  $ED_{50}$  is an average fluence determined from the  $ED_{50}$  in terms of energy divided by the area calculated from the spot size area. Three or four separate data collection sets are shown for each melanosome fraction.

Sample type	$ED_{50}$ ( $\text{J/cm}^2$ )	Lower fiducial limits (FL) ( $\text{J/cm}^2$ )	Upper fiducial limits (FL) ( $\text{J/cm}^2$ )	Probit slope	Number of shots
HB	0.577	0.515	0.627	9.9	111
	0.641	0.603	0.697	18.1	106
	0.590	0.561	0.617	13.6	152
LB	0.636	0.608	0.657	25.3	97
	0.516	0.452	0.563	11.9	78
	0.589	0.552	0.630	25.6	96
HP	0.580	0.531	0.625	14.0	79
	0.605	0.578	0.633	15.9	91
	0.630	0.587	0.670	21.9	88
LP	0.645	0.597	0.690	20.9	67
	0.623	0.595	0.657	23.3	129
	0.645	0.597	0.720	20.6	68
	0.620	0.582	0.647	33.6	99

related to a decrease in melanosome absorption coefficients with increasing wavelengths, as shown in Sec. 5.2. The error bars in Fig. 3 represent the 95% fiducial confidence limits determined with Probit analysis. However, as previously reported, the overall variability and experimental uncertainty of the measured fluence at the  $ED_{50}$  values is estimated to be  $\pm 16\%$ .

Table 5 is a comparison of the 532-nm, 10-ns threshold data with similar visible nanosecond pulse melanosome thresholds from various authors.<sup>6,7,20,32</sup> The threshold values of  $99.2$  and  $97.4 \text{ mJ/cm}^2$  are reported as average fluence, whereas

**Table 2** Probit threshold data for the combined trials for single pulse duration of 10 ns for HB, HP, LB and LP of melanosomes at 1100 nm. For each melanosome fraction, data points taken on successive days were analyzed using Probit to provide a single  $ED_{50}$  value. The  $1/e^2$  Gaussian beam diameter average was  $183 \mu\text{m}$ . The reported  $ED_{50}$  is an average fluence determined from the  $ED_{50}$  in terms of energy divided by the area calculated from the spot size area.

Sample type	$ED_{50}$ ( $\text{J/cm}^2$ )	Lower FL ( $\text{J/cm}^2$ )	Upper FL ( $\text{J/cm}^2$ )	Probit slope	Number of shots
HB	0.603	0.583	0.624	12.9	369
LB	0.608	0.590	0.624	13.2	478
HP	0.618	0.598	0.638	17.1	307
LP	0.623	0.605	0.642	24.7	296

**Table 3** Probit threshold data for the combined trials for single pulse durations of 50 ns for HB, HP, LB, and LP fractions of melanosomes at 1319 nm. Similar to Table 2, the 1319 nm data taken on successive days was combined in order to produce a single ED<sub>50</sub> threshold value. The 1/e<sup>2</sup> Gaussian beam diameter average was 183 μm. The reported ED<sub>50</sub> is an average fluence determined from the ED<sub>50</sub> in terms of energy divided by the area calculated from the spot size area.

Sample type	ED <sub>50</sub> (J/cm <sup>2</sup> )	Lower FL (J/cm <sup>2</sup> )	Upper FL (J/cm <sup>2</sup> )	Probit slope	Number of shots
HB	2.68	2.63	2.74	14.1	656
LB	2.61	2.55	2.68	12.7	577
HP	2.7	2.64	2.76	13.2	654
LP	2.63	2.56	2.69	11.2	667

Brinkmann et al.<sup>7</sup> and Neumann and Brinkmann<sup>6,32</sup> report peak fluence. In addition, average fluence values from Kelly<sup>20</sup> are reported. The average fluence values from this current study are in the range of previous reported values. Peak fluence was determined from the bovine and porcine average fluence, resulting in values of 198.4 and 194.8 mJ/cm<sup>2</sup>, respectively, as a comparison to the values reported in Table 5.

## 5.2 Melanosome Absorption Coefficients

Melanosome absorption coefficients were calculated from the threshold values found in Fig. 3. A first-order estimate of the melanosome absorption coefficient,  $\mu_m$ , as a function of threshold fluence,  $F_{th}(T)$ , measured at melanosome temperature T can be obtained using the equation of Brinkmann et al.<sup>7</sup>

$$T_{th} - T = [\mu_m F_{th}(T)] / [C_p \rho]. \quad (4)$$

Here  $C_p$  is the melanosome specific heat,  $\rho$  is the melanosome density, and  $T_{th}$  is the threshold temperature for bubble formation. From Ref. 6, the melanosome-specific heat and

**Table 4** Probit threshold data for all wavelengths collected. At each wavelength, data for both heavy and light melanosome fractions were combined into a single Probit average threshold fluence for bovine and porcine melanosomes.

Sample type	Wavelength (nm)	ED <sub>50</sub> (J/cm <sup>2</sup> )	Lower FL (J/cm <sup>2</sup> )	Upper FL (J/cm <sup>2</sup> )	Probit slope	Number of shots
Bovine		0.514	0.504	0.523	18.3	706
Porcine	1000	0.497	0.488	0.506	24.9	521
Bovine		0.606	0.592	0.619	13.1	847
Porcine	1100	0.620	0.607	0.633	19.8	603
Bovine		0.833	0.819	0.848	18.5	634
Porcine	1200	0.842	0.826	0.859	18.2	468
Bovine		2.650	2.610	2.690	13.4	1233
Porcine	1319	2.660	2.620	2.710	12.0	1321

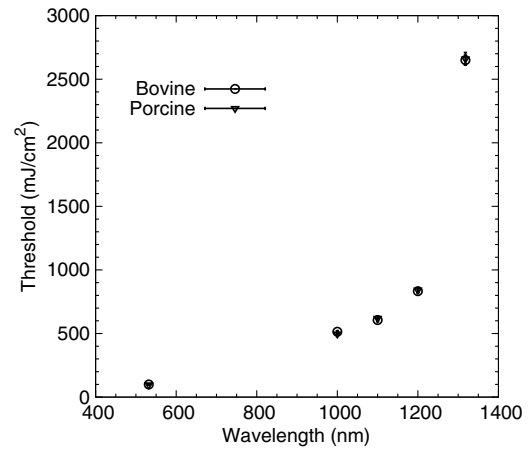


**Fig. 3** Comparison of fluence threshold and wavelength of bovine and porcine melanosomes on a linear scale from 532 to 1319 nm. Error bars represent the upper and lower 95% fiducial confidence intervals. There are no statistical differences between the two species of melanosomes.

particle density are  $C_p = 2.55$  J/gm-C and  $\rho = 1.41$  gm/cm<sup>3</sup>. Threshold fluences were measured at ambient temperature of  $T = 20^\circ\text{C}$ , and for this first-order calculation, an estimated threshold temperature of  $T_{th} = 150^\circ\text{C}$  was used based on the temperature-dependent, nanosecond pulse, melanosome microcavitation studies of Kelly<sup>20</sup> and Neumann and Brinkmann.<sup>6</sup> Averaging the bovine and porcine data from Table 4, the fluence thresholds were 0.506 J/cm<sup>2</sup> (1000 nm), 0.613 J/cm<sup>2</sup> (1100 nm), 0.838 J/cm<sup>2</sup> (1200 nm), and 2.655 J/cm<sup>2</sup> (1319 nm). Using these in Eq. (4), and solving for  $\mu_m$ , yields melanosome absorption coefficients of 925 cm<sup>-1</sup> (1000 nm), 763 cm<sup>-1</sup> (1100 nm), 558 cm<sup>-1</sup> (1200 nm), and 176 cm<sup>-1</sup> (1319 nm). Table 6 shows the NIR absorption coefficients for melanosomes and are compared to RPE coefficients based on a fit to data extrapolated from data in Birngruber et al.<sup>14</sup> The estimated uncertainty for

**Table 5** Threshold comparisons at 532 and 565 nm with single, nanosecond exposures from various authors. The uncertainty presented in this table for the present study represents the fiducial limits determined by Probit analysis. Brinkmann (Ref. 7) and Neumann (Refs. 6 and 32) report peak fluence values, while Kelly (Ref. 20) and the present study values represent an average fluence.

Pulse width (ns)	Wavelength (nm)	Threshold fluence (mJ/cm <sup>2</sup> )	Fluence	Sample type	Reference
8	532	90	Peak	Porcine	7
12	532	117 ± 28	Peak	Porcine	32
12	532	139	Peak	Porcine	6
20	532	55 ± 5	Average	Bovine	20
20	565	110 ± 5	Average	Bovine	20
10	532	99.2 ± 6	Average	Bovine	Present study
10	532	97.4 ± 7	Average	Porcine	Present study

**Table 6** A comparison of the retinal pigmented epithelium (RPE) and melanosome absorption coefficients ( $\mu_m$ ) as a function of wavelength. The RPE values were based on a fit to data extrapolated from Birngruber et al. (Ref. 14). The uncertainty was estimated by combining the experimental uncertainty of  $F_{th}$  and the threshold temperature ( $T_{th}$ ) variability from Refs. 6, 7, and 32.

Wavelength (nm)	RPE ( $\text{cm}^{-1}$ )	Melanosome ( $\text{cm}^{-1}$ )	Melanosome uncertainty ( $\text{cm}^{-1}$ )
532	1381	4718	$\pm 896$
1000	161	925	$\pm 176$
1100	102	736	$\pm 140$
1200	64	558	$\pm 106$
1319	41	176	$\pm 33$

the melanosome absorption coefficients in Table 6 is the result of the combined experimental  $ED_{50}$  threshold error and the uncertainty in the threshold temperature bubble formation ( $T_{th}$ ) range reported by various authors.<sup>6,7,32</sup> An additional method to determine absorption coefficients can be performed according to Gerstman et al.<sup>10</sup> In this case, Mie scattering effects are neglected, and the internal absorption coefficient of an RPE melanosome can be calculated, resulting in a homogeneous absorption coefficient. Neumann and Brinkmann<sup>6</sup> used this method to compare the measured absorption efficiency of RPE melanosomes to absorption coefficients reported by other authors. The resulting homogeneous absorption coefficients are in reasonable agreement with absorption coefficients of melanosomes found in previous studies.<sup>6</sup> The method used in this study to estimate absorption coefficients are within the range of previously reported RPE melanosome absorption coefficients at 532 nm found in Ref. 6 as well as the calculated coefficients based on Gerstmann et al.<sup>10</sup>

The NIR absorption coefficients for melanosomes and RPE are plotted in Fig. 4, along with the water absorption on a log

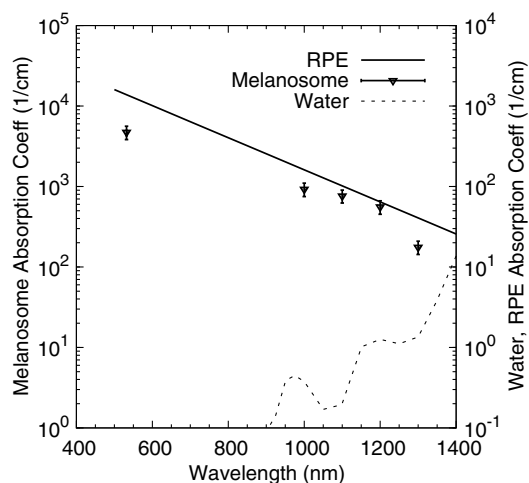


**Fig. 4** Absorption coefficients on log scale with water comparison, curve of retinal pigmented epithelium (RPE) data from Birngruber et al. (Ref. 14) at 532 to 1400 nm. Although the magnitude is different between RPE and melanosome coefficients, the overall relative trend of decreasing value with increasing wavelength is observed.

scale. While the granular absorption coefficients are an order of magnitude higher than the corresponding layer values, the results indicate that the relative changes in absorption coefficient as a function of wavelength are similar. The absorption coefficient of the melanosomes also remains much larger than that of water, indicating that microcavitation should be possible beyond 1319 nm.

## 6 Discussion

### 6.1 Microcavitation Thresholds

This paper documents the first reported measurements of melanosome microcavitation threshold data for single, nanosecond-duration laser pulses in the 1 to 1.3  $\mu\text{m}$  wavelength region. Melanosome microcavitation in the RPE is believed to be the threshold level ocular damage mechanism for sub-microsecond-duration laser exposures in the visible and NIR. These NIR microcavitation data are especially relevant at this time because of a recent proposal to modify the ANSI Z136.1 safety standards in the NIR. Supporting data are needed for this proposal, not only on ocular damage thresholds, but also on ocular damage mechanisms and trends.

Results indicate that there is no significant difference in absorption characteristics between melanosome fractions even though there are slight shape and size differences between heavy and light melanosomes based on the separation method used for these experiments. Results also indicate that there is a significant increase in NIR threshold values with increasing wavelength, but no significant difference between bovine and porcine melanosomes. In addition, 532-nm data were collected and compared to previous reports from other authors. The threshold value obtained was in the midrange of previously published values, indicating that the data presented here are similar to those collected by other researchers. These data validate the threshold range presented in this paper in the NIR wavelength region.

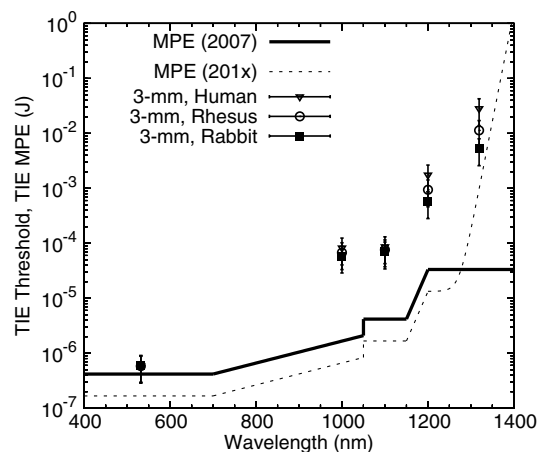


**Fig. 5** Comparison of ANSI Z136.1-2007 and proposed ANSI Z136.1-201x exposure limits for 1 to 100 ns pulses, expressed in terms of permissible total intraocular energy (TIE). Estimated threshold is based upon a 3-mm-diameter ( $1/e^2$ ) Gaussian beam entering a human, rhesus, or rabbit eye, respectively. The estimated uncertainty of 51% was determined from  $\pm 0.25$  diopter, retinal transmission uncertainty, and energy measurement uncertainty.

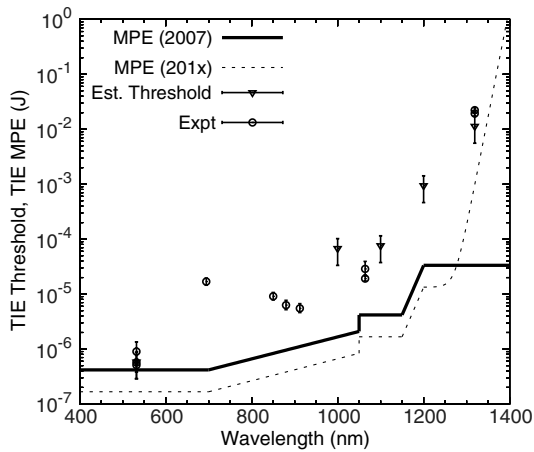


**Fig. 6** Comparison of ANSI Z136.1-2007 and proposed ANSI Z136.1-201x exposure limits for 1 to 100 ns pulses, expressed in terms of permissible TIE. Estimated threshold is based upon a 3-mm-diameter ( $1/e^2$ ) Gaussian beam entering a rhesus eye. Experimental data are from referenced sources in Table 7 (Refs. 34 to 41), including a number of differing beam diameters to the eye, but rhesus subjects.

## 6.2 Melanosome Absorption Coefficients

The data of Fig. 3 show a nonlinear increase in microcavitation fluence threshold with increasing wavelength, especially in the transition between 1200 and 1300 nm. A fivefold decrease was calculated in the melanosome absorption coefficient between 1000 and 1319 nm based on the microcavitation threshold data and the model of Brinkmann et al.,<sup>7</sup> as shown in Table 6 and Fig. 4. While the melanosome absorption coefficients are much higher than the corresponding RPE layer values, the data trends are similar to those of the RPE absorption coefficients. Results were compared to the RPE layer absorption coefficients in the NIR due to the lack of NIR melanosome

coefficient data. Two different material absorption trends influence ocular absorption and ocular damage in this region. First, water absorption increases dramatically above 1050 nm, reducing light transmission to the retina and producing a shift from retinal to corneal damage at longer optical wavelengths (seen in Fig. 4). Second, there is a significant decrease in the melanosome absorption coefficient as wavelengths increase from the visible into the mid-IR. Thus, these data confirm the trends in absorption coefficients with increasing wavelength.

## 6.3 Total Intraocular Energy Trends and MPE Levels

In order to determine the validity of melanosome cavitation threshold values, estimated retinal spot size and ocular transmission values were calculated for rhesus monkey, rabbit, and human eyes based on the model of Vincette et al.,<sup>18</sup> and fluence threshold values from this experiment were used to calculate the energy (in joules) needed to cause retinal damage in this regime. Since the exact energy reaching the retina is unknown, retinal damage thresholds are typically reported as the total intraocular energy (TIE), which is the energy delivered to the corneal plane resulting in retinal damage. Furthermore, estimates of TIE help determine the energy that produces minimum visible lesions (MVLs). In this study, estimates for the retinal beam diameter were based on the TIE from a 3-mm-diameter ( $1/e^2$ ) Gaussian beam entering an emmetropic eye, which is typical of experimental data. Figure 5 compares the TIE values of the three species, based on the transmission to the retina, to the current and proposed MPE levels. In each case, the average threshold values at each studied wavelength were used to determine the TIE damage values. Error bars for the estimated TIE values represent  $\sim 51\%$  uncertainty, based on a  $\pm 0.25$  diopter deviation from emmetropia, uncertainty in retinal transmission, and uncertainty in energy measurements.<sup>33</sup> Figure 5 indicates that as wavelength increases, the changes in transmission to

**Table 7** Comparison of *in vivo* ED<sub>50</sub> TIE values from 532 to 1319 nm in the nanosecond pulse regime, and a range of corneal irradiance diameters. These data are plotted in Fig. 6 and compared with estimated threshold values in the same wavelength regime (Refs. 34 to 41).

Wavelength (nm)	Pulse duration (ns)	Corneal irradiance diameter (mm)	Damage site	Observation time (h)	ED <sub>50</sub> TIE ( $\mu$ J)	Range ( $\mu$ J)	Reference
532	4	2.5	Retina	24	0.90	0.6 to 1.35	34
532	3.5	3	Retina	24	0.51	0.38 to 0.65	35
532	3.5	6	Retina	24	0.57	0.29 to 0.79	36
694.3	30	3	Retina	1	16.90	14.5 to 19.6	37
850.2	11		Retina	1	9.10	7.8 to 10.7	38
880	14		Retina	1	6.30	5.2 to 7.7	38
912	7		Retina	1	5.50	4.6 to 6.7	38
1064	7	3	Retina	1	28.70	22.3 to 39.3	39
1064	7	3	Retina	24	19.10	17.3 to 21.2	40
1319	50	4.5	Retina	24	19,300	17,300 to 21,200	41
1319	50	4.5	Retina	24	22,000	20,100 to 24,600	41

the retina vary with species, resulting in significantly different TIE values at 1319 nm. Figure 5 also shows all but the TIE values at 532 nm well above the current MPE levels (solid line). Figure 5 also includes the proposed MPE levels (dashed line) for the new ANSI standard<sup>2</sup> to show that a sufficient margin of safety is maintained across the retinal hazard regime. These data support the proposed lowering of MPE levels at 532 nm, as well as the proposed increase in MPE levels at 1300 nm.

Figure 6 further compares estimated TIE thresholds for the rhesus eye (based on a 3 mm beam diameter) to *in vivo* nanosecond experimental studies in the rhesus eye, with differing beam diameters over the wavelength range from 532 to 1319 nm.<sup>34–41</sup> As shown, the trends in the estimated values from the fluence thresholds determined in this study mimic the trends in the MVL studies of several authors. The uncertainty for the *in vivo* measurements corresponds to the upper and lower fiducial limits found in Table 7. Table 7 reports *in vivo* results in the nanosecond pulse duration from 532 to 1319 nm for rhesus monkey subjects.

Trends in melanosome microcavitation fluence thresholds determined in this study are comparable to estimated and experimental TIE thresholds from 532 to 1319 nm. Both experimental data and estimated threshold values based on single melanosome microcavitation events indicate that the proposed changes to the MPE values are adequate. This study indicates that threshold measurements at 532 nm could potentially overlap with the 2007 MPE levels. In addition, this study provides data that support the increase in MPE levels at 1300 nm. This report validates the proposed changes to the MPE levels.

## 7 Conclusions

This research investigated trends in single melanosome microcavitation thresholds for nanosecond pulses in the NIR (1000 to 1319 nm) wavelength regime. While many studies have been reported for visible nanosecond pulse melanosome microcavitation, NIR nanosecond microcavitation has been neglected. This study reports the first threshold values for NIR nanosecond pulse melanosome microcavitation, as well as the first reported values for NIR melanosome absorption coefficients.

Melanosome microcavitations were observed through strobe microscopy, and fluence threshold values were determined through Probit analysis. Results indicated that as the laser wavelength increased, the ED<sub>50</sub> threshold values also increased nonlinearly with a factor of ~25 times lower at 532 nm than at 1319 nm. In addition, results follow trends in bulk RPE layer absorption reported by other authors. There is a significant increase in threshold values at 1319 nm compared to 1200 nm. No statistical differences were seen between thresholds for bovine and porcine melanosomes, and no differences were observed between the heavy and light melanosomes. The latter indicates that slight size variations do not significantly affect melanosome laser energy absorption. The nonlinear increase in NIR threshold appears to be primarily due to a corresponding decrease in melanosome absorption coefficients with increasing wavelength. Calculations indicated a fivefold decrease in the melanosome absorption coefficient between 1000 and 1319 nm. This trend was found to be comparable to the decrease in RPE layer absorption coefficients over the same wavelength region. Estimated TIE values were calculated based on melanosome microcavitation fluence thresholds, and they agree with published *in vivo* MVL studies. Estimated

TIE values were also compared to current and proposed MPE values, and these data support the proposed revisions to the safety standard MPEs in the 532 to 1400 nm wavelength region.

## Acknowledgments

This research was supported in part while Morgan Schmidt was appointed to the Postgraduate Research Participation Program at the Air Force Research Laboratory, 711th Human Performance Wing, Bioeffects Division, Optical Radiation Bioeffects Branch administered by the Oak Ridge Institute for Science and Education through an interagency agreement between the U.S. Department of Energy and AFRL. In addition, this research was performed in part while Morgan Schmidt held a National Research Council Research Associateship at AFRL.

## References

1. American National Standards Institute, "American National Standard for safe use of lasers," 2007, [http://www.lia.org/PDF/Z136\\_1\\_s.pdf](http://www.lia.org/PDF/Z136_1_s.pdf) (12 February 2014).
2. ICNIRP, "ICNIRP guidelines on limits of exposure to incoherent visible and infrared radiation," *Health Phys.* **105**(1), 74–96 (2013).
3. R. L. Vincelette et al., "Trends in retinal damage thresholds from 100-millisecond near-infrared laser radiation exposures: a study at 1,110, 1,130, 1,150, and 1,319 nm," *Lasers Surg. Med.* **41**(5), 382–390 (2009).
4. J. A. Zuclich, D. J. Lund, and B. E. Stuck, "Wavelength dependence of ocular damage thresholds in the near-IR to far-IR transition region: proposed revisions to MPEs," *Health Phys.* **92**(1), 15–23 (2007).
5. C. P. Lin and M. W. Kelly, "Cavitation and acoustic emission around laser-heated microparticles," *Appl. Phys. Lett.* **72**(22), 2800–2802 (1998).
6. J. Neumann and R. Brinkmann, "Boiling nucleation on melanosomes and microbeads transiently heated by nanosecond and microsecond laser pulses," *J. Biomed. Opt.* **10**(2), 024001 (2005).
7. R. Brinkmann et al., "Origin of retinal pigment epithelium cell damage by pulsed laser irradiance in the nanosecond to microsecond time regimen," *Lasers Surg. Med.* **27**(5), 451–464 (2000).
8. C. P. Lin et al., "Selective cell killing by microparticle absorption of pulsed laser radiation," *IEEE J. Sel. Topics Quantum Electron.* **5**(4), 963–968 (1999).
9. B. A. Rockwell, R. J. Thomas, and A. Vogel, "Ultrashort laser pulse retinal damage mechanisms and their impact on thresholds," *Med. Laser Appl.* **25**(2), 84–92 (2010).
10. B. S. Gerstman et al., "Laser-induced bubble formation in the retina," *Surg. Med.* **18**(1), 10–21 (1996).
11. H. Lee et al., "Optical detection of intracellular cavitation during selective laser targeting of the retinal pigment epithelium: dependence of cell death mechanism on pulse duration," *J. Biomed. Opt.* **12**(6), 064034 (2007).
12. J. Neumann and R. Brinkmann, "Cell disintegration by laser-induced transient microbubbles and its simultaneous monitoring by interferometry," *J. Biomed. Opt.* **11**(4), 041112 (2006).
13. D. H. Sliney and M. L. Wolbarsht, *Safety with Lasers and Other Optical Sources*, Plenum Press, New York (1980).
14. R. Birngruber, F. Hillenkamp, and V. P. Gabel, "Theoretical investigations of laser thermal retinal injury," *Health Phys.* **48**(6), 781–796 (1985).
15. R. Brinkmann, J. Roeder, and R. Birngruber, "Selective retina therapy (SRT): a review on methods, techniques, preclinical and first clinical results," *Bulletin de la Societe Belge d'Ophthalmologie* **302**, 51–69 (2006).
16. C. P. Cain et al., "Porcine skin visible lesion thresholds for near-infrared lasers including modeling at two pulse durations and spot sizes," *J. Biomed. Opt.* **11**(4), 041109 (2006).
17. R. L. Vincelette et al., "First-order model of thermal lensing in a virtual eye," *J. Opt. Soc. Am. A Opt. Image Sci. Vis.* **26**(3), 548–558 (2009).
18. R. L. Vincelette et al., "Thermal lensing in ocular media exposed to continuous-wave near-infrared radiation: the 1150–1350-nm region," *J. Biomed. Opt.* **13**(5), 054005 (2008).

19. D. J. Payne et al., "Comparative study of laser damage threshold energies in the artificial retina," *J. Biomed. Opt.* **4**(3), 337–334 (1999).
20. M. W. Kelly, "Intracellular cavitation as a mechanism of short-pulse laser injury to the retinal pigment epithelium," PhD Dissertation, Tufts University, Medford, Massachusetts (1997).
21. I. A. Vitkin et al., "Optical and thermal characterization of natural (*Sepia officinalis*) melanin," *Photochem. Photobiol.* **59**(4), 455–462 (1994).
22. M. H. Niemz, *Laser-Tissue Interactions Fundamentals and Applications*, Springer, New York (1996).
23. D. Leszczynski et al., "Laser-beam-triggered microcavitation: a novel method for selective cell destruction," *Radiat. Res.* **156**(4), 399–407 (2001).
24. E. Faraggi and B. S. Gerstman, "Acoustical resonant absorption of pulsed laser radiation by a spherical absorber," *J. Appl. Phys.* **102**(12), 123505 (2007).
25. G. Schuele et al., "RPE damage thresholds and mechanisms for laser exposure in the microsecond-to-millisecond time regimen," *Invest. Ophthalmol. Vis. Sci.* **46**(2), 714–719 (2005).
26. J. Roegner, R. Brinkmann, and C. P. Lin, "Pump-probe detection of laser-induced microbubble formation in retinal pigment epithelium cells," *J. Biomed. Opt.* **9**(2), 367–371 (2004).
27. A. Vogel and V. Venugopalan, "Mechanisms of pulsed laser ablation of biological tissues," *Chem. Rev.* **103**(2), 557–644 (2003).
28. E.-A. Brujan and A. Vogel, "Stress wave emission and cavitation bubble dynamics by nanosecond optical breakdown in a tissue phantom," *J. Fluid Mech.* **558**, 281–308 (2006).
29. A. E. Dontsov, R. D. Glickman, and M. A. Ostrovsky, "Retinal pigment epithelium pigment granules stimulate the photo-oxidation of unsaturated fatty acids," *Free Radic. Biol. Med.* **26**(11–12), 1436–1446 (1999).
30. C. P. Cain and G. D. Noojin, "A comparison of various probit methods for analyzing yes/no data on a log scale," AL/OE-TR-1996-0102, USAF Armstrong Laboratory (1996).
31. D. J. Finney, *Probit Analysis*, Cambridge University Press, New York, NY (1971).
32. J. Neumann and R. Brinkmann, "Nucleation dynamics around single microabsorbers in water heated by nanosecond laser irradiation," *J. Appl. Phys.* **101**(11), 114701 (2007).
33. D. H. Sliney et al., "What is the meaning of threshold in laser injury experiments? Implications for human exposure limits," *Health Phys.* **82**(3), 335–347 (2002).
34. C. P. Cain et al., "Visible retinal lesions from ultrashort laser pulses in the primate eye," *Invest. Ophthalmol. Vis. Sci.* **36**(5), 879–888 (1995).
35. B. J. Lund, D. J. Lund, and P. R. Edsall, "Laser-induced retinal damage threshold measurements with wavefront correction," *J. Biomed. Opt.* **13**(6), 064011 (2008).
36. B. J. Lund, D. J. Lund, and P. R. Edsall, "Damage threshold from large retinal spot size repetitive-pulse laser exposures," in *Int. Laser Safety Conf.*, Paper #302, Laser Institute of America (2009).
37. E. S. Frisch, G. D. Beatrice, and R. C. Holsen, "Comparative study of argon and ruby retinal damage thresholds," *Invest. Ophthalmol. Vis. Sci.* **10**(11), 911–919 (1971).
38. D. J. Lund, E. S. Beatrice, and S. T. Schuschereba, "Bioeffects data concerning the safe use of GaAs laser training devices," in *Combat Ocular Problems*, E. S. Beatrice, Ed., pp. 15–29, Letterman Army Institute of Research, San Francisco, California (1982).
39. C. P. Cain et al., "Thresholds for visible lesions in the primate eye produced by ultrashort near-infrared laser pulses," *Invest. Ophthalmol. Vis. Sci.* **40**(10), 2343–2349 (1999).
40. C. P. Cain et al., "Visible lesion thresholds from near-infrared pico and nanosecond laser pulses in the primate eye," *Proc. SPIE* **2975**, 133–137 (1997).
41. J. A. Zuclich et al., "Ocular effects and safety standard implications for high-power lasers in the 1.3–1.4  $\mu\text{m}$  wavelength range," USAF Technical Report no. AFRL-HE-BR-TR- 2004-0187, pp. 1–16, AFRL/HEDO, San Antonio (2004).

Biographies of the authors are not available.